

# Primordial black hole formation in the early universe: critical behaviour and self-similarity

Ilia Musco<sup>1</sup> and John C. Miller<sup>2,3</sup>

<sup>1</sup>Centre of Mathematics for Applications, Department of Mathematics, University of Oslo, PO Box 1053 Blindern, NO-0316 Oslo, Norway

<sup>2</sup>Department of Physics (Astrophysics), University of Oxford, Keble Road, Oxford OX1 3RH, UK

<sup>3</sup>SISSA, International School for Advanced Studies, Via Bonomea 265, I-34136 Trieste, Italy

**Abstract.** Following on after three previous papers discussing the formation of primordial black holes during the radiative era of the early universe, we present here a further investigation of the critical nature of the process involved, aimed at making contact with some of the basic underlying ideas from the literature on critical collapse. We focus on the intermediate state, which we have found appearing in cases with perturbations close to the critical limit, and examine the connection between this and the similarity solutions which play a fundamental role in the standard picture of critical collapse. We have derived a set of self-similar equations for the null-slicing form of the metric which we are using for our numerical calculations, and have then compared the results obtained by integrating these with the ones coming from our simulations for collapse of cosmological perturbations within an expanding universe. We find that the similarity solution is asymptotically approached in a region which grows to cover both the contracting matter and part of the semi-void which forms outside it. Our main interest is in the situation relevant for primordial black hole formation in the radiative era of the early universe, where the relation between the pressure  $p$  and the energy density  $e$  can be reasonably approximated by an expression of the form  $p = we$  with  $w = 1/3$ . However, we have also looked at other values of  $w$ , both because these have been considered in previous literature and also because they can be helpful for giving further insight into situations relevant for primordial black hole formation. As in our previous work, we have started our simulations with initial supra-horizon scale perturbations of a type which could have come from inflation.

PACS numbers: 04.70.-s, 98.80.Cq

Submitted to: *Class. Quantum Grav.*

## 1. Introduction

A population of primordial black holes (PBHs) might have been formed in the early universe due to gravitational collapse of sufficiently large-amplitude cosmological perturbations. Following the initial papers suggesting this (Zel'dovich & Novikov (1969) [1]; Hawking (1971) [2]; Carr & Hawking (1974) [3]; and Carr (1975) [4]), various authors then investigated the process numerically (Nadezhin, Novikov & Polnarev (1978) [5]; Bicknell & Henriksen (1979) [6]; Novikov & Polnarev (1980) [7]; Niemeyer and Jedamzik (1999) [8]; Shibata and Sasaki (1999) [9]; Hawke & Stewart (2002) [10]; Musco, Miller & Rezzolla (2005) [11]). In order to form a PBH, the perturbation would need to have an amplitude  $\delta$  greater than a certain threshold value  $\delta_c$  (with  $\delta$  often being defined as the relative mass excess inside the overdense region, measured at the time of horizon crossing). The numerical investigations clarified many different aspects of the nature of the process, with particular reference to the radiative era of the universe (with the equation of state being taken as  $p = \frac{1}{3}e$ , where  $p$  is the pressure and  $e$  is the energy density). This context represents the most commonly studied scenario for PBH formation.

Niemeyer & Jedamzik (1999) [8, 12] showed that the masses of PBHs produced in the radiative era by perturbations of a given profile type, follow the typical scaling-law behaviour of critical collapse, first discovered for idealized circumstances by Choptuik (1993) [14], i.e. the masses of the black holes produced follow a power law  $M_{BH} \propto (\delta - \delta_c)^\gamma$  if  $\delta$  is close enough to  $\delta_c$ . Neilsen & Choptuik (2000) [15] later showed that one could get a critical collapse, using a succession of “imploding shells” of matter as the initial conditions, for  $p = we$  equations of state with any value of  $w$  in the range  $0 - 1$ . They found that the value of the critical exponent  $\gamma$  was dependent only on the value of  $w$  and not on the particular form of the perturbation profile.

In 2002, Hawke & Stewart [10] returned to the problem of PBH formation in the early universe, with  $w = 1/3$ , and investigated the nature of the collapse going down to smaller values of  $(\delta - \delta_c)$  than Niemeyer & Jedamzik had been able to do with their code. For the larger values of  $(\delta - \delta_c)$ , comparable with those of [8], Hawke & Stewart again found a scaling law with a similar value of  $\gamma$ , but for smaller  $(\delta - \delta_c)$  they saw formation of strong shocks and their curve of  $\log M_{BH}$  against  $\log(\delta - \delta_c)$  flattened off at a minimum mass of around  $10^{-3}$  of their horizon mass. They also found that the value of  $\delta_c$  depended strongly on the shape of the perturbation, in contrast to [8].

In Musco et al (2005) [11], we considered PBH formation with initial conditions given by very small linear perturbations of the energy density and velocity fields approximating the growing components of cosmological perturbations, and imposed with a length-scale much larger than that of the cosmological horizon. The domination of the growing component becomes even greater by the time of horizon crossing, as any residual decaying component dies away. We again saw a scaling law with similar  $\gamma$  for the range of values of  $(\delta - \delta_c)$  used in [8] but found very different values of  $\delta_c$  from [8] for similar perturbation shapes (we were concentrating on those types of perturbation).

This difference was attributed to the fact that in [8], the perturbations were made just in the energy density and were imposed directly at the horizon scale, so that their value of  $\delta_c$  was calculated with inclusion of a substantial decaying component which did not then contribute to the black hole formation. If one focuses on the effect of perturbations originating from inflation, then clearly only growing components will be relevant at much later times.

In Polnarev & Musco (2007) [16], this kind of cosmologically-relevant initial perturbation was imposed in a more precise way, using an asymptotic quasi-homogeneous solution [17]. Starting from a curvature perturbation, which is a time-independent quantity when the perturbation length-scale is much larger than the cosmological horizon [18], perturbations in all of the other quantities can then be specified in a consistent way, giving a solution with only a growing component. The metric perturbation can be large even when the perturbations in energy density and velocity are small, and only when there is a large-amplitude metric perturbation, corresponding to a non-linear initial perturbation of the curvature, can one get  $\delta > \delta_c$  at horizon crossing.

In Musco et al (2009) [19], we returned to the issue raised by Hawke & Stewart [10] concerning whether the scaling law would continue down to very small values of  $(\delta - \delta_c)$ . In order to address this, we needed to modify our code with the inclusion of adaptive mesh refinement (AMR) so as to be able to handle the extreme conditions which arise near to the critical limit. In view of our earlier work, we were particularly wanting to investigate the effect of using initial perturbations with just a growing component imposed on a scale larger than the horizon, rather than the non-linear sub-horizon scale initial perturbations used in [10]. We again used the quasi-homogeneous solution to provide our initial conditions. Doing this, we did not observe the shock formation seen in [10] (which we attributed to the presence of a non-linear decaying component in their calculations) but instead found that regular scaling-law behaviour was preserved all the way down to the vicinity of the resolution limit of our scheme (going beyond the most extreme values shown in [10]). A striking feature of our calculations was the appearance of an “intermediate state” for cases near to the critical limit. For these cases, when the over-dense region detaches from the rest of the universe, it reaches a compactness  $2M/R \sim 0.5$  (where  $R$  and  $M$  are its current radius and mass) at which it then remains while proceeding to contract, shedding matter as it shrinks in such a way as to maintain  $2M/R$  roughly unchanging (with just a small gradual decrease). This situation (the “intermediate state”) persists through many e-foldings if  $\delta$  is very close to  $\delta_c$ . Eventually, it reaches a mass at which it either enters a final collapse phase leading to black hole formation, or disperses into the surrounding medium.

The existence of a similarity solution for cases near to the critical limit, is a key feature in the theory of critical collapse [20, 21], and in [19] we saw some evidence of self-similarity also in the context of PBH formation within an expanding universe, associated with the intermediate state. In that paper, however, we were mainly focusing on the issue of preservation of the scaling-law. Here, instead, we focus on the issue of

self-similarity, aiming to clarify the extent to which our intermediate-state solution does follow a self-similar behaviour. As a secondary point, we also report on calculations which we have made for values of  $w$  different from  $1/3$ , using the same approach. Although these other values are of less interest from a physical point of view, they have been considered previously in the critical-collapse literature, and it can be useful to study them using the same approach so as to get further insight into the main case of interest. Also, this can be useful for indicating what may happen at epochs of the universe at which the equation of state softens due to phase transitions.

For the work of this paper, we have used the same numerical code as in [19], but with some fine tuning of the AMR. Following the present Introduction, section 2 reviews our mathematical formulation of the problem and presents the self-similar equations as they appear when written in the null-slicing foliation used for our numerical calculations. Solutions of the self-similar equations are also presented there. Section 3 contains a brief summary of the numerical methods used for the simulations. In section 4, we make comparison between the simulation results and the similarity solution, and section 5 discusses the changes in the values of  $\gamma$  and  $\delta_c$  which come from varying  $w$  and the shape of the initial perturbation. Section 6 contains conclusions. Throughout, we use units for which  $c = G = 1$ .

## 2. Mathematical formulation of the problem

### 2.1. Cosmic-time slicing

For the calculations described here, we have followed the same basic methodology as described in our previous papers [11, 16, 19] (which we will refer to as Papers 1, 2 and 3 respectively). We therefore give just a brief summary of it here; more details are contained in the previous papers.

We use two different formulations of the general relativistic hydrodynamic equations: one for setting the initial conditions and the other for studying the black hole formation. Throughout, we are assuming spherical symmetry and that the medium can be treated as a perfect fluid; we use a Lagrangian formulation of the equations with a radial coordinate  $r$  which is co-moving with the matter.

For setting the initial conditions, it is convenient to use a diagonal form of the metric, with the time coordinate  $t$  reducing to the standard Friedmann-Robertson-Walker (FRW) time in the case of a homogeneous medium with no perturbations. (This sort of time coordinate is therefore often referred to as “cosmic time”). We write this metric in the form given by Misner & Sharp [22] (but with a change in notation for the metric coefficients):

$$ds^2 = -a^2 dt^2 + b^2 dr^2 + R^2 (d\theta^2 + \sin^2 \theta d\varphi^2) , \quad (1)$$

with  $a$ ,  $b$  and  $R$  being functions of  $r$  and  $t$  and with  $R$  playing the role of an Eulerian radial coordinate. We follow the Misner-Sharp approach for writing the GR

hydrodynamic equations. Using the notation

$$D_t \equiv \frac{1}{a} \left( \frac{\partial}{\partial t} \right), \quad (2)$$

$$D_r \equiv \frac{1}{b} \left( \frac{\partial}{\partial r} \right), \quad (3)$$

one defines the quantities

$$U \equiv D_t R, \quad (4)$$

and

$$\Gamma \equiv D_r R, \quad (5)$$

where  $U$  is the radial component of four-velocity in the ‘‘Eulerian’’ frame and  $\Gamma$  is a generalized Lorentz factor. The metric coefficient  $b$  can then be written as

$$b \equiv \frac{1}{\Gamma} \frac{\partial R}{\partial r}. \quad (6)$$

With these specifications, the GR hydrodynamic equations can be written in the following form (with the notation that  $e$  is the energy density,  $p$  is the pressure,  $\rho$  is the compression factor and  $M$  is the mass contained inside radius  $R$ ):

$$D_t U = - \left[ \frac{\Gamma}{(e+p)} D_r p + \frac{M}{R^2} + 4\pi R p \right], \quad (7)$$

$$D_t \rho = - \frac{\rho}{\Gamma R^2} D_r (R^2 U), \quad (8)$$

$$D_t e = \frac{e+p}{\rho} D_t \rho, \quad (9)$$

$$D_t M = -4\pi R^2 p U, \quad (10)$$

$$D_r a = - \frac{a}{e+p} D_r p, \quad (11)$$

$$D_r M = 4\pi R^2 \Gamma e, \quad (12)$$

plus a constraint equation

$$\Gamma^2 = 1 + U^2 - \frac{2M}{R}. \quad (13)$$

An equation of state is also needed, and we are here considering ones of the form

$$p = w e, \quad (14)$$

with  $w$  being a constant.

## 2.2. Initial conditions

a perturbation of the otherwise uniform medium representing the cosmological background solution, with the length-scale of the perturbation  $R_0$  being much larger than the cosmological horizon  $R_H \equiv H^{-1}$ . Under these circumstances, the perturbations in  $e$  and  $U$  can be extremely small while still giving a large-amplitude perturbation of the metric (as is necessary if a black hole is eventually to be formed) and the above system of equations can then be solved analytically to first order in the small parameter  $\epsilon \equiv (R_H/R_0)^2 \ll 1$ . A full discussion of this has been given in Paper 2. The result obtained, referred to as the “quasi-homogeneous solution”, gives formulae for the perturbations of all of the metric and hydrodynamical quantities in terms only of a curvature perturbation profile  $K(r)$ , where  $r$  is the co-moving radial coordinate linked to  $R$  by  $R = S(t)r$  with  $S(t)$  being the FRW scale factor;  $K(r)$  is conveniently time-independent when  $\epsilon \ll 1$  [18].

To characterize the amplitude of the perturbation, we use the integrated quantity

$$\delta(t) = \left( \frac{4}{3} \pi r_0^3 \right)^{-1} \int_0^{r_0} 4\pi r^2 \left( \frac{e(r,t) - e_b(t)}{e_b(t)} \right) dr, \quad (15)$$

which measures the relative mass excess within the overdense region, as frequently done in the literature;  $e_b$  is the background value of the energy density and  $r_0$  is the co-moving length-scale of the overdense region of the perturbation. In Paper 2 (to which we refer for details) it was shown that

$$\frac{e(r,t) - e_b(t)}{e_b(t)} \equiv \delta e(r,t) = \epsilon(t) \frac{3(1+w)}{5+3w} \frac{r_0^2}{3r^2} \frac{\partial [r^3 K(r)]}{\partial r}, \quad (16)$$

and here we consider the initial curvature profile  $K(r)$  introduced in Paper 2<sup>‡</sup>

$$K(r) = \left( 1 + \alpha \frac{r^2}{2\Delta^2} \right) \exp \left( -\frac{r^2}{2\Delta^2} \right), \quad (17)$$

which implies

$$K'(r) = \frac{r}{\Delta^2} \left[ \alpha - \left( 1 + \alpha \frac{r^2}{2\Delta^2} \right) \right] \exp \left( -\frac{r^2}{2\Delta^2} \right). \quad (18)$$

Inserting  $K(r)$  and  $K'(r)$  into (16) one gets

$$\delta e(r,t) = \epsilon(t) \frac{3(1+w)}{5+3w} r_0^2 \left[ \left( 1 + \alpha \frac{r^2}{2\Delta^2} \right) \left( 1 - \frac{r^2}{3\Delta^2} \right) + \alpha \frac{r^2}{3\Delta^2} \right] \exp \left( -\frac{r^2}{2\Delta^2} \right). \quad (19)$$

The relation between  $r_0$  and  $\Delta$  for a given  $K(r)$ , is obtained by putting to zero the expression inside the square brackets with  $r$  set equal to  $r_0$ . This gives

$$r_0^2 = f(\alpha) \Delta^2, \quad (20)$$

where

<sup>‡</sup> The equations as presented here include corrections of some typographical errors in the equations of Paper 2 which have already been noted in Paper 3.

$$f(\alpha) = \begin{cases} 3 & \text{if } \alpha = 0 \\ \frac{(5\alpha - 2) + \sqrt{(5\alpha - 2)^2 + 24\alpha}}{2\alpha} & \text{if } \alpha \neq 0 \end{cases} \quad (21)$$

Fixing the parameter  $\alpha$  selects a particular perturbation profile, with the simplest choice being given by  $\alpha = 0$ , corresponding to a Gaussian curvature profile  $K(r)$

$$K(r) = \exp\left(-\frac{3}{2}\left(\frac{r}{r_0}\right)^2\right), \quad (22)$$

which gives a Mexican hat profile for the energy density perturbation  $\delta e(r, t)$ , as often used in the literature [8, 11, 19]:

$$\delta e(r, t) = \epsilon(t) \frac{9(1+w)}{5+3w} \Delta^2 \left(1 - \frac{r^2}{3\Delta^2}\right) \exp\left(-\frac{r^2}{2\Delta^2}\right). \quad (23)$$

The perturbation shape is fixed by the choice of  $\alpha$ , while the perturbation amplitude is determined by the value chosen for  $\Delta$ . Inserting (19) into (15) one gets

$$\delta(t) = \epsilon(t) \frac{3(1+w)}{5+3w} f(\alpha) \Delta^2 \left(1 + \alpha \frac{f(\alpha)}{2}\right) \exp\left(-\frac{f(\alpha)}{2}\right), \quad (24)$$

within the linear regime, where  $\epsilon \ll 1$ , with the time evolution of the perturbation being given by  $\epsilon(t)$ , which measures how the perturbation length-scale  $R_0$  changes with respect to the cosmological horizon scale  $R_H$ . The expression for  $\epsilon(t) = (R_H/R_0)^2$  involves only background quantities for the unperturbed universe and inserting this gives

$$\delta(t) = \delta(t_i) \left(\frac{t}{t_i}\right)^{\frac{2(1+3w)}{3(1+w)}}, \quad (25)$$

which leads to the familiar relationships  $\delta(t) \propto t$  when  $w = 1/3$  and  $\delta(t) \propto t^{2/3}$  when  $w = 0$ .

For our discussion here, we need a value for  $\delta$  measured in a standard way, and it is convenient to use for this the value given by taking  $\epsilon(t) = 1$  in (24). For small perturbations, this value for  $\delta$  coincides with the one at the horizon-crossing time, and it does not differ by very much from that even for the larger perturbations of interest for PBH formation, at least for the types of perturbation profile being used here. Since evaluating (24) analytically in this way is much more precise than making a numerical integral on the grid at horizon-crossing time, we use this value here, as we did in Papers 2 and 3.

### 2.3. Null slicing

In our work, the Misner-Sharp approach, with cosmic time slicing, has been used for setting the initial conditions and then for evolving them to produce corresponding initial conditions on an outgoing null slice. These are then passed to the main code which uses the “observer time” null-slicing formulation of Hernandez & Misner [24] for following the further evolution leading up to black hole formation. In this formulation, each outgoing null slice is labelled with a time coordinate  $u$ , which takes a constant value everywhere on the slice, and the metric (1) is re-written as

$$ds^2 = -f^2 du^2 - 2fb dr du + R^2 (d\theta^2 + \sin^2 \theta d\varphi^2) , \quad (26)$$

where  $f$  is the new lapse function which determines how the value of  $u$  changes from one slice to another. The lapse  $f$  needs to be normalised by setting  $u$  equal to the proper time of some suitable observer, and the standard way of doing this is to equate it to the proper time of a distant observer, as we have done in our previous papers (setting  $f = 1$  at the location of that observer). However, this is not suitable for our present discussion of the connection with similarity solutions, because distant observers are not within the region covered by the similarity solution. Because of this, we instead synchronise here with the proper time of a central observer, setting  $f = 1$  at  $r = 0$ .

Within this formulation, the operators equivalent to (2) and (3) are

$$D_t \equiv \frac{1}{f} \left( \frac{\partial}{\partial u} \right) , \quad (27)$$

$$D_k \equiv \frac{1}{b} \left( \frac{\partial}{\partial r} \right) , \quad (28)$$

where  $D_k$  is the radial derivative in the null slice and the corresponding derivative in the Misner-Sharp space-like slice is given by

$$D_r = D_k - D_t . \quad (29)$$

The hydrodynamic equations can then be formulated in a way analogous to what was done in cosmic time. The system of equations used in the main code, replacing the cosmic-time ones (7) – (12), are:

$$D_t U = -\frac{1}{1 - c_s^2} \left[ \frac{\Gamma}{(e + p)} D_k p + \frac{M}{R^2} + 4\pi R p + c_s^2 \left( D_k U + \frac{2U\Gamma}{R} \right) \right] , \quad (30)$$

$$D_t \rho = \frac{\rho}{\Gamma} \left[ D_t U - D_k U - \frac{2U\Gamma}{R} \right] , \quad (31)$$

$$D_t e = \left( \frac{e + p}{\rho} \right) D_t \rho , \quad (32)$$

$$D_k \left[ \frac{(\Gamma + U)}{f} \right] = -4\pi R \left( \frac{e + p}{f} \right) , \quad (33)$$

$$D_t M = -4\pi R^2 p U , \quad (34)$$



$$D_k M = 4\pi R^2 [e\Gamma - pU], \quad (35)$$

where  $c_s = \sqrt{(\partial p / \partial e)}$  is the sound speed. § The quantity  $\Gamma$  is given by (13), as before, and we also have

$$\Gamma = D_k R - U, \quad (36)$$

which replaces equation (5) in this slicing.

#### 2.4. Self-similarity: equations and solution

In this paper, we are wanting to investigate the connection between our numerical calculations for gravitational collapse of cosmological perturbations within the expanding medium of the early universe, and studies by previous authors looking at the problem of critical collapse under simpler circumstances (in particular, with asymptotic flatness) where the presence of similarity solutions plays a key role. There, as  $(\delta - \delta_c) \rightarrow 0$ , one approaches a critical solution where all of the matter in the original contracting region is shed during the contraction which ends, with zero matter, at a time referred to as the critical time  $t_c$ . The later stages of this follow a similarity solution. For small positive values of  $(\delta - \delta_c)$ , the similarity solution is closely approached but eventually there is a divergence away from it, with the remaining material collapsing to form a black hole. In our previous calculations, we have noted the appearance of an “intermediate state” during which the behaviour gave some indication of being roughly self-similar. Here, we are wanting to investigate this in more detail in order to understand how closely this reproduces what was seen in the previous critical collapse work. For doing this, we first needed to derive the equations governing the similarity solutions in the Hernandez-Misner foliation, as used for our numerical calculations.

Our self-similar coordinate  $\xi$  is the ratio between the distance away from the centre of symmetry and the time away from the critical time, both of which are given in terms of invariantly-defined quantities. For the distance, we use the circumferential radius  $R$  and for the time we use the outgoing null time  $u$  with the lapse  $f$  set equal to 1 at the centre, so that  $u$  is synchronized with the proper time of a central observer. (Note that this approach is importantly different from that of Evans & Coleman [20] who normalised the time differently and obtained a more complicated form for their similarity solution.) For deriving the hydrodynamical equations in self-similar form, it is convenient to set the zero point of the time scale to be at the critical time. The times being considered are ones before the critical time and hence take negative values; we then define our self-similar coordinate, which needs to be positive, as

$$\xi \equiv -\frac{R}{u}, \quad (37)$$

and look for a solution of the system of partial differential equations of the previous section in terms of quantities depending only on  $\xi$ . For that set of quantities we have

§ Note that there was a typographical error in equation (27) of Paper 1; equation (33) here is the correct form which has been used throughout for the calculations in all of our papers.

$U$ ,  $\Gamma$  and  $f$ , as already defined, and two new ones:  $\Omega \equiv 4\pi R^2 e$  and  $\Phi \equiv M/R$ , while we eliminate  $\rho$  by combining equations (31) and (32), and write the pressure  $p$  in terms of the energy density  $e$  using the equation of state  $p = we$  (which gives the sound-speed  $c_s = \sqrt{w}$ ). To derive the self-similar form of the equations, we then proceed as follows. First, we write the Hernandez-Misner equations in an ‘‘Eulerian’’ form, using coordinates  $R$  and  $u$ . For a general quantity  $Y$ , we have

$$dY = \left( \frac{\partial Y}{\partial u} \right)_R du + \left( \frac{\partial Y}{\partial R} \right)_u dR, \quad (38)$$

which then gives

$$\begin{aligned} \left( \frac{\partial Y}{\partial u} \right)_r &= \left( \frac{\partial Y}{\partial u} \right)_R + \left( \frac{\partial Y}{\partial R} \right)_u \left( \frac{\partial R}{\partial u} \right)_r, \\ &\rightarrow \left( \frac{\partial Y}{\partial u} \right)_R + fU \left( \frac{\partial Y}{\partial R} \right)_u, \end{aligned} \quad (39)$$

inserting the expression for  $U \equiv D_t R$ . Similarly

$$\begin{aligned} \left( \frac{\partial Y}{\partial r} \right)_u &= \left( \frac{\partial Y}{\partial R} \right)_u \left( \frac{\partial R}{\partial r} \right)_u, \\ &\rightarrow b(\Gamma + U) \left( \frac{\partial Y}{\partial R} \right)_u \end{aligned} \quad (40)$$

inserting the expression for  $\Gamma \equiv D_r R$ . The operators  $D_t$  and  $D_k$  can therefore be written in the Eulerian form

$$D_t \equiv \frac{1}{f} \left( \frac{\partial}{\partial u} \right)_r = \frac{1}{f} \left( \frac{\partial}{\partial u} \right)_R + U \left( \frac{\partial}{\partial R} \right)_u, \quad (41)$$

$$D_k \equiv \frac{1}{b} \left( \frac{\partial}{\partial r} \right)_u = (\Gamma + U) \left( \frac{\partial}{\partial R} \right)_u, \quad (42)$$

which, combined with the definition of the self-similar coordinate  $\xi$ , gives

$$D_t = \frac{1}{R} \left( U + \frac{\xi}{f} \right) \frac{d}{d \ln \xi}, \quad (43)$$

$$D_k = \frac{1}{R} (\Gamma + U) \frac{d}{d \ln \xi}, \quad (44)$$

One then finds that equations (13), (30) - (35) can indeed be recast as a system for  $U$ ,  $\Omega$ ,  $\Phi$ ,  $f$  and  $\Gamma$ , depending only on  $\xi$ . After a considerable amount of algebra, we arrive at a set of three ordinary differential equations

$$\frac{d \ln U}{d \ln \xi} = \left[ \frac{(\Phi + w\Omega)^2 - 2w\Gamma^2\Phi}{U^2(\Phi + w\Omega)^2 - w\Gamma^2(\Omega - \Phi)^2} \right] \left[ (\Omega - \Phi) - \frac{(1+w)\Omega U}{(\Gamma + U)} \right] \quad (45)$$

$$\frac{d \ln \Omega}{d \ln \xi} = \frac{(1+w)(\Omega - \Phi)}{(\Phi + w\Omega)} \frac{d \ln U}{d \ln \xi} + \frac{2w}{(\Phi + w\Omega)} \left[ (\Omega - \Phi) - \frac{(1+w)\Omega U}{(\Gamma + U)} \right] \quad (46)$$

$$\frac{d \ln \Phi}{d \ln \xi} = \frac{1}{\Phi} \left[ (\Omega - \Phi) - \frac{(1+w)\Omega U}{(\Gamma + U)} \right] \quad (47)$$

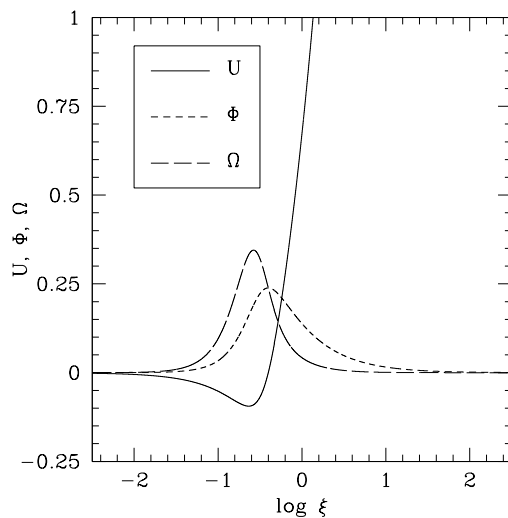


**Figure 1.** The self-similar solutions in null time for  $U$ ,  $\Phi$  and  $\Omega$  plotted against  $\log \xi$  for  $w = 1/3$ .

together with two algebraic equations

$$\Gamma = 1 + U^2 - 2\Phi, \quad (48)$$

$$f = -\frac{\xi}{(1+w)\Omega U} \left[ (\Omega - \Phi) - \frac{U}{\Gamma}(\Phi + w\Omega) \right]. \quad (49)$$

Note that the three ODEs do not depend explicitly on the lapse  $f$ . However,  $U$ ,  $\Omega$  and  $\Phi$  all require a boundary condition. Clearly they all go to zero at  $R = 0$ , and hence at  $\xi = 0$ , but since the equations involve derivatives with respect to  $\ln \xi$ , we need to series-expand away from  $\xi = 0$  in order to start our integration. To get the expression for  $U$ , it is necessary to specify the central value of  $f$  which, as already mentioned, we are setting equal to 1. For small  $\xi$ , we then find

$$\left\{ \begin{array}{l} U(\xi) = -\frac{2}{3(1+w)}\xi \\ \Phi(\xi) = k\xi^2 \\ \Omega(\xi) = 3k\xi^2 \end{array} \right. \quad (50)$$

to lowest order in  $\xi$ , with the constant  $k$  being determined by requiring regularity of the solution for  $U$  at the critical point, where the numerator and denominator of the first term on the right hand side of equation (45) both go to zero.

The integration of equations (45) - (47) was carried out using a fourth-order Runge-Kutta scheme, with a shooting method being used to determine the value of  $k$ . Since  $U$  can be negative, the derivative  $d \ln U / d \ln \xi$  needs to be re-written as  $(1/U) dU / d \ln \xi$  when performing the integration. Results are shown in figure 1 where  $U$ ,  $\Omega$  and  $\Phi$  are plotted as functions of  $\log \xi$  for  $w = 1/3$ .

### 3. The method used for the numerical simulations

The present calculations for PBH formation have been made with the same code as used in Paper 3. Since this has been fully described previously, we will just give a brief outline of it here. It is an explicit Lagrangian hydrodynamics code based on that of Miller & Motta (1989) [25] but with the grid organized in a way similar to that of Miller & Rezzolla (1995) [26] which was designed for calculations in an expanding cosmological background. The code has a long history and has been carefully tested in its various forms. The basic grid uses logarithmic spacing in a mass-type comoving coordinate, allowing it to reach out to very large radii while giving finer resolution at small radii. Our initial data is derived from the quasi-homogeneous solution and is specified on a space-like slice (at constant cosmic time) with  $\epsilon = 10^{-2}$ , giving  $R_0 = 10 R_H$ . The outer edge of the grid has here been placed at  $1000 R_H$  for convenience in making some of the plots; putting it at  $90 R_H$ , as we did previously, was already sufficient for ensuring that there is no causal contact between it and the perturbed region during the time of the calculations. The initial data is then evolved using the Misner-Sharp equations (7-13), so as to generate a second set of initial data on a null slice and the null-slice initial data is then evolved using the Hernandez-Misner equations (see [11]).

For the calculations presented in Paper 3, we introduced an adaptive mesh refinement scheme (AMR), on top of the existing logarithmic grid, giving us sufficient resolution so as to be able to follow black hole formation down to extremely small values of  $(\delta - \delta_c)$ . Having the AMR is particularly important for allowing us to follow the deep voids which form outside the central contracting region in cases very close to the critical limit. The same scheme has been used with just minor modifications for the calculations presented here. Our aim in writing the AMR was to avoid the use of artificial viscosity, but it has now emerged that some residual artificial viscosity was still present and is necessary for correct functioning of the code in its present form. The presence of this is not thought to affect the results presented in any important way, however. We have successfully used the scheme with more than thirty levels of refinement and all relevant features of the solutions have been fully resolved.

### 4. Comparison between the simulation results and the similarity solution

In this section, we present results from our investigation of the extent to which the “intermediate state” seen previously in our numerical simulations corresponds to the similarity solution discussed in section 2.4. First, we recall the background to this coming from our earlier work.

At the beginning of our calculations, we have a growing perturbation, with a length-scale larger than the cosmological horizon, consisting of a slight over-density which is expanding along with the rest of the universe but a little more slowly. After it enters within the cosmological horizon, it starts to contract and then collapse if its amplitude  $\delta$  is large enough. As described earlier, if  $\delta$  is greater than the critical value  $\delta_c$ , it goes

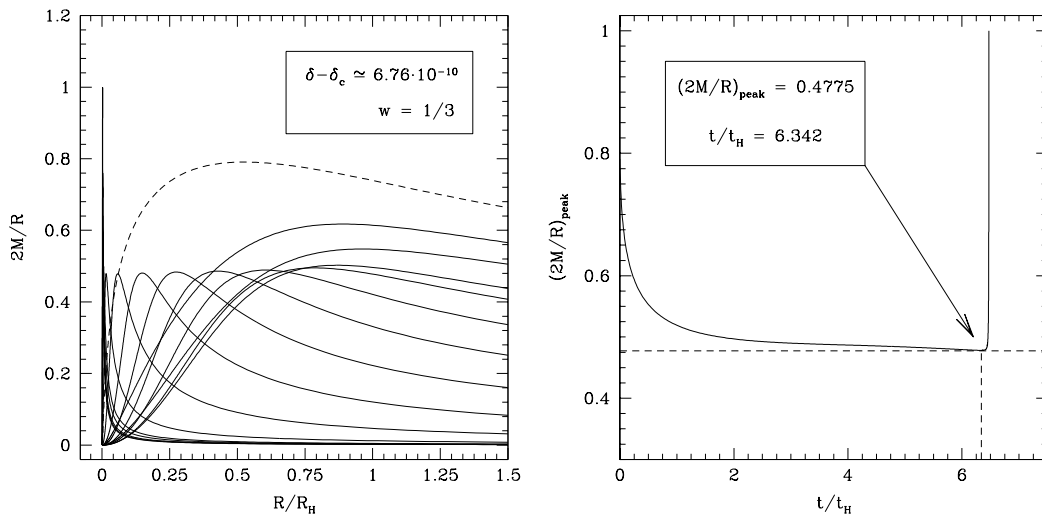


**Figure 2.** In the left-hand frame, we show the behaviour of  $2M/R$  for a nearly critical case plotted against  $R/R_H$  at different time levels, where  $R_H$  is the cosmological horizon scale at the moment of horizon crossing. The dashed curve indicates the initial conditions used by the null-time code. The right-hand frame shows the time evolution of the peak of  $2M/R$  during the intermediate state with  $t/t_H$  being the null time (normalised in the same way as for the similarity solution) measured in units of the horizon crossing time  $t_H (= R_H/2)$ . The horizontal dashed line indicates the value of  $(2M/R)_{\text{peak}}$  coming from the corresponding similarity solution, while the vertical dashed line indicates when the intermediate state ends for this case, very close to the critical time. In the collapse following this,  $(2M/R)_{\text{peak}}$  increases rapidly towards 1 with the formation of the black hole.

on to produce a black hole, while for smaller values it eventually disperses into the background medium. Initially, the over-dense region has decreasing compactness  $2M/R$  but, if  $\delta$  is only slightly greater than  $\delta_c$ , it then reaches a value of  $2M/R$  at which it remains with very little change as it proceeds to contract, shedding matter as it shrinks in such a way as to keep  $2M/R$  roughly constant (but with just a small continuing gradual decrease). For a radiation fluid with  $w = 1/3$ , this “intermediate state” has  $2M/R \sim 0.5$ , quite far from the condition for a black hole. A large pressure gradient develops at the edge of the contracting matter and it is this which drives the wind, opening up a deep void between the contracting matter and the rest of the universe. Eventually, there is a deviation away from the intermediate state and  $2M/R$  increases towards 1. This process was investigated in detail in Paper 3 for a radiation fluid with  $w = 1/3$  and some evidence was seen of self-similar behaviour during the period of the intermediate state. We investigate this further here. Throughout this section, we consider only  $w = 1/3$  and, since we are dealing with an astrophysical application, we use  $t$  to denote time even when we are dealing with the null time previously denoted by  $u$ .

For making our discussion, we focus on a particular case near to the critical

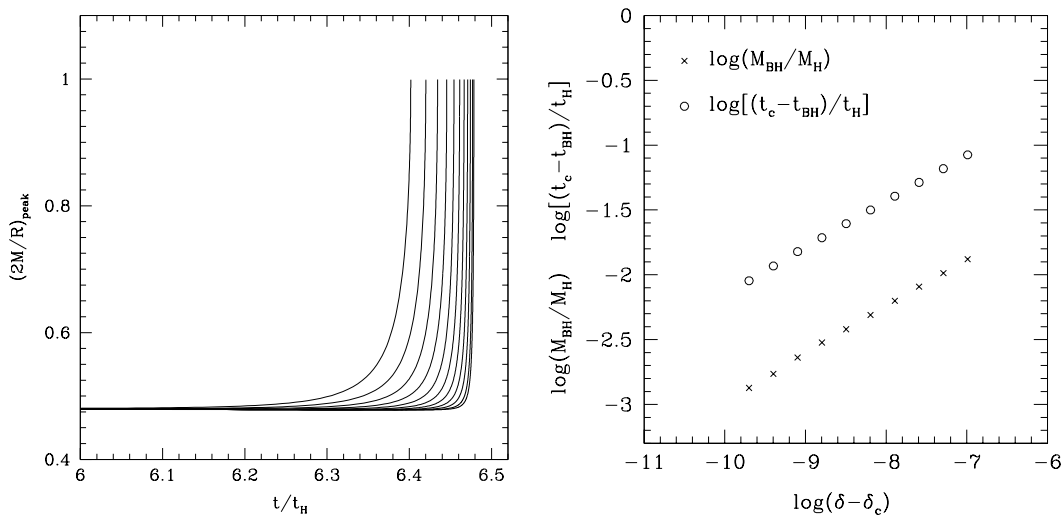


**Figure 3.** In the left-hand frame,  $(2M/R)_{\text{peak}}$  is plotted as a function of time for a succession of values of  $(\delta - \delta_c)$  equally spaced in the log, showing the convergence of the black-hole formation time  $t_{\text{BH}}$  as  $(\delta - \delta_c)$  is reduced. The right-hand frame shows the scaling-law behaviour of  $M_{\text{BH}}/M_H$  and  $(t_c - t_{\text{BH}})/t_H$  as a function of  $(\delta - \delta_c)$ .

threshold, starting from a standard Mexican hat perturbation in the energy density (i.e.  $\alpha = 0$ ) with  $(\delta - \delta_c) = 6.76 \times 10^{-10}$ . This gives rise to a black hole with mass  $2.14 \times 10^{-3} M_H$ , where  $M_H$  is the cosmological horizon mass at the horizon-crossing time. The left-hand frame of figure 2 shows the behaviour of  $2M/R$  plotted against  $R/R_H$  at different time levels for this case ( $R_H$  being the cosmological horizon scale at the moment of horizon crossing). The dashed curve shows the initial conditions used by the null-time code. The subsequent evolution proceeds in the direction of decreasing  $(2M/R)_{\text{peak}}$  until the intermediate state is reached, and then the peak moves progressively inwards. When  $\delta$  is extremely close to the critical limit, as it is here, the intermediate state with almost constant  $(2M/R)_{\text{peak}}$ , persists through many e-foldings and the eventual turn-off away from it, with  $(2M/R)_{\text{peak}}$  rising towards the black-hole value of 1, happens very abruptly.

Another view of this behaviour is shown in the right-hand frame of figure 2, where the time evolution of  $(2M/R)_{\text{peak}}$  is plotted, from the same run as shown in the left-hand frame, again starting the plot from the time of the initial data for the null-time code. The time coordinate used is normalised as described above. The horizontal dashed line shows the value of  $(2M/R)_{\text{peak}}$  coming from the similarity solution (corresponding to the peak of  $\Phi$  in figure 1 – note that  $(2M/R) = 2\Phi$ ). In the simulation, the peak starts from a fairly high value after the perturbation has re-entered the cosmological horizon, and then decreases while the overdense region continues expanding along with the rest of the universe. Eventually the expansion of the overdense region reverses, and  $(2M/R)_{\text{peak}}$  settles into the roughly-constant value of the intermediate state, approaching the similarity value more and more closely as time goes on. It is almost

touching the similarity line at the moment when the intermediate state ends and the rapid collapse towards black-hole formation begins. The behaviour is roughly similar for the other values of  $w$  which we have tested (in connection with the discussion in the next section). The intermediate state lasts for longer with smaller values of  $w$  and the similarity value of  $(2M/R)_{\text{peak}}$  changes with  $w$  in such a way as to remain roughly equal to  $\delta_c$ .

In figure 3, the left-hand frame is a zoom of a series of curves similar to that in the right-hand frame of figure 2, but drawn for a succession of values of  $(\delta - \delta_c)$ , equally-spaced in the log, decreasing from left to right. It can be seen that, as  $(\delta - \delta_c)$  decreases, the rising part of the curve becomes progressively more abrupt and the value of  $t$  when  $(2M/R)_{\text{peak}} \rightarrow 1$  (which we will call  $t_{BH}$ ) is tending towards a limiting value  $t_c$  as  $\delta \rightarrow \delta_c$ . This is the critical time needed for comparing with the similarity solutions, with  $\xi$  for the simulation results set equal to  $R/(t_c - t)$ . As can be seen from the right-hand frame,  $(t_c - t_{BH})$  again follows a scaling law in  $(\delta - \delta_c)$  which has the same value of the exponent as for the black hole masses (also plotted here).

If the similarity solution were being followed exactly, the central energy density would scale with time as  $(t_c - t)^{-2}$  (this follows from the behaviour of  $\Omega$  given in equation (50)). An alternative way of obtaining a value for  $t_c$  is therefore to fit this scaling to the simulation results. This is less precise than the limiting procedure discussed above (because the similarity solution is only being followed approximately) but the value obtained for  $t_c$  in this way agrees with the previous one to around one part in  $10^4$  if the time-variation at the closest approach to the similarity solution is used.

Figures 4 and 5, which use data from the same run as in figure 2, show in detail how the simulation results for the intermediate state approach the similarity solution. Quantities from the simulation are plotted against the similarity coordinate  $\xi$  for a succession of times during the intermediate state (the first being for  $t/t_H = 5.072$  and the last being for  $t/t_H = 6.342$  which is just before  $(2M/R)_{\text{peak}}$  starts to increase). Figure 4 shows three different views of the velocity  $U$ , with the bottom frame being a zoom of the top left-hand one, looking at the range of  $U \leq 1$ ; figure 5 shows  $2M/R$  ( $= 2\Phi$ ) and  $\Omega$  ( $= 4\pi R^2 e$ ). The later times correspond to the lower curves on the right-hand side of the plots and to the upper curves in the mid-region of the frames in figure 4. The similarity solutions of figure 1 are shown here with short-dashed curves, but these are often covered. One can see the progressive approach of the simulation results towards the similarity solutions, with the range of the zone of agreement increasing with time. At the last time shown, the similarity solution is closely approximating the simulation results over all of the contracting region, where  $U$  is negative, and also over the part of the surrounding region out to the maximum of  $U$  (the peak of the relativistic wind which coincides with the minimum of the energy density in the evacuated region - see figure 4 of Paper 3). Beyond this, the simulation results diverge completely away from the similarity solution, eventually merging into the surrounding FRW universe. The top right-hand frame of figure 4 shows the last of the time levels seen in the previous frame, together with the short-dashed curve for the similarity solution and a

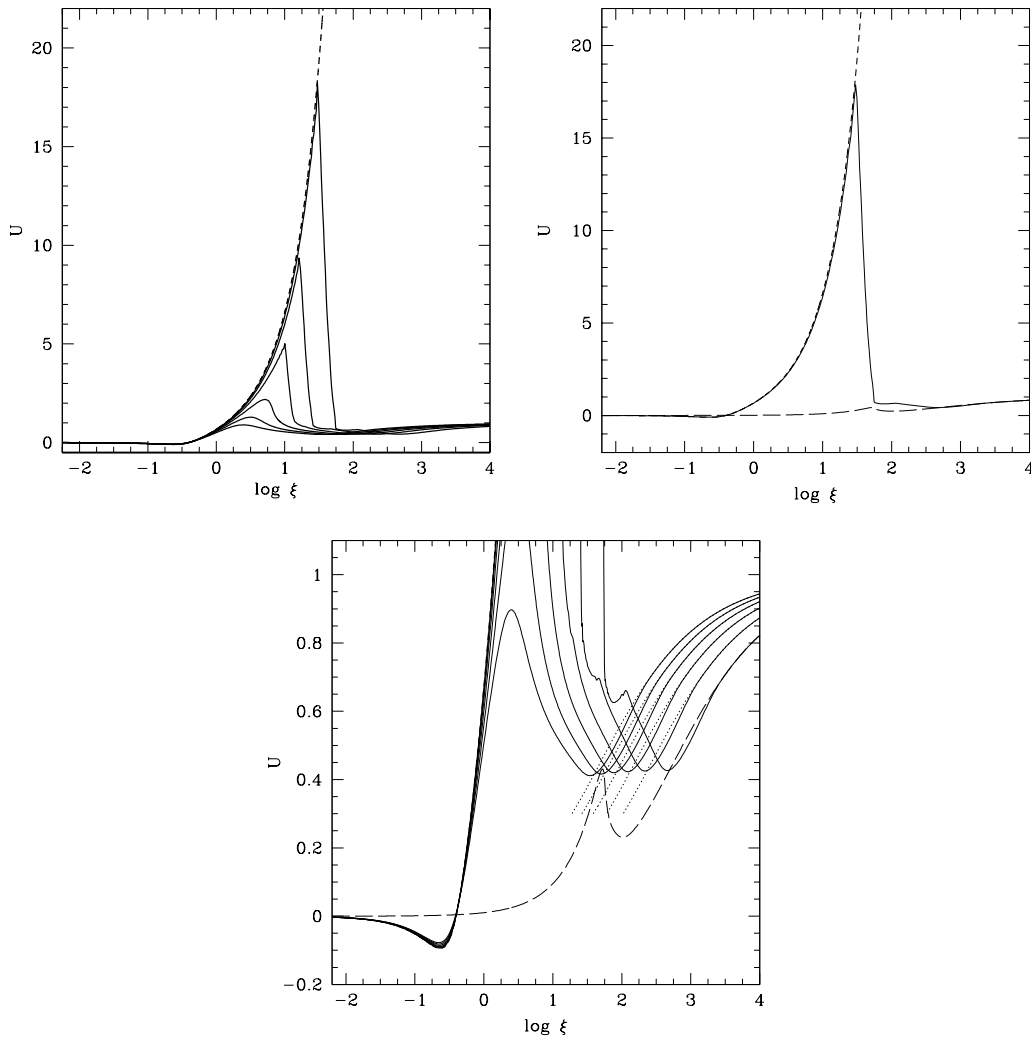


**Figure 4.** Simulation results for the velocity  $U$  (from the same run as in figure 2) plotted against the similarity coordinate  $\xi$ . The top left-hand frame shows curves for a succession of times during the intermediate state (the higher peaks corresponding to the later ones). The similarity solution is marked with the short-dashed curve. The top right-hand frame shows only the last of these time levels, but together with a long-dashed curve indicating the unperturbed FRW solution mapped onto this same space-time slice. The bottom frame is a zoom of the first one, looking in detail at the range  $U \leq 1$ . The long-dashed curve marks the same mapping of the FRW solution as before and the truncated dotted lines show part of the corresponding mappings for the earlier time levels. See text for further details.

long-dashed curve indicating the unperturbed FRW solution mapped onto this same space-time slice. (This curve has been obtained by calculating the local value of the Hubble constant  $H = 1/2t_{\text{pr}}$ , where  $t_{\text{pr}}$  is proper time as measured by the local co-moving observers, and then taking  $U = HR$ .) In the bottom frame, with the expanded view for  $U \leq 1$ , the long-dashed curve again shows the mapping of the FRW solution



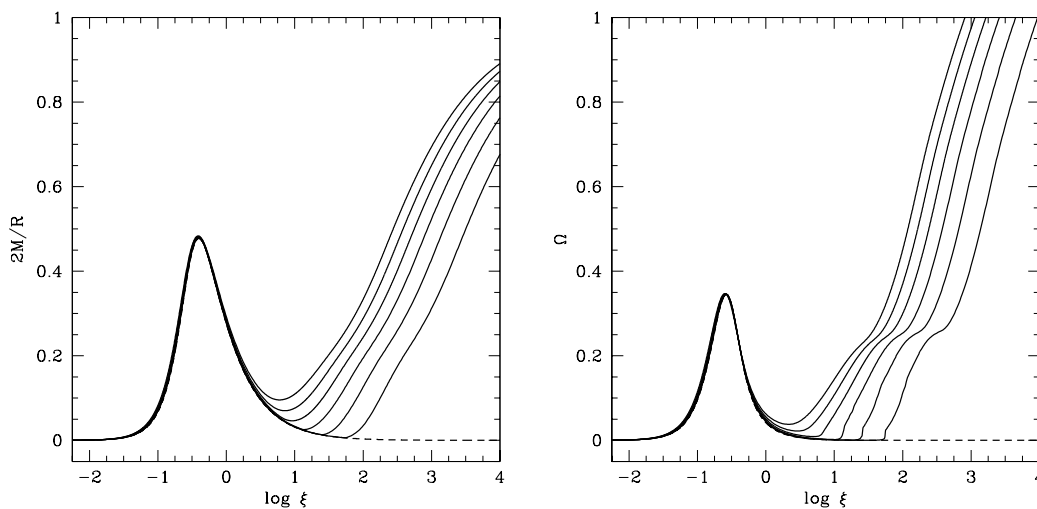


**Figure 5.** Corresponding simulation results (to those of the previous figure) for  $2M/R (= 2\Phi)$  and  $\Omega (= 4\pi R^2 e)$ . The similarity solutions are again marked with the short-dashed curves.

onto the same space-time slice as before and the truncated dotted lines show part of the corresponding curves for the earlier time levels. Note that the strange form of the long-dashed curve arises because of the perturbation of the null slice onto which the FRW solution is being mapped. The join between the computed solution and the FRW solution in the outer region comes at the same locations, of course, also in the plots of figure 5 and excellent agreement is found there between the numerical and analytic results in all cases.

Regarding figure 4, we should stress that the use of a logarithmic coordinate here has the effect of making features appear much more abrupt than they would with a standard linear coordinate. The almost vertical parts of the curves in the top frames are nowhere near to being shocks and correspond to smoothly-varying features when viewed on a linear scale (c.f. figure 4 of Paper 3). The zoomed bottom frame has been primarily included so as to show clearly the transition to the FRW solution. However, it also reveals an interesting wave-like feature at the later times (seen in the solid curves), which we have then investigated in more detail. This turns out to result from interaction of the wind with the outer edge of the growing void and appears as a rather gentle space-variation when viewed on a linear scale.

From the right-hand frame of figure 2, showing the intermediate state during which the numerical results are very close to those coming from the similarity solution (as seen in figures 4 and 5), it is very clear that there is a systematic behaviour in the approach of the numerical solution to the self-similar one. There is also a systematic behaviour in the eventual departure from the similarity solution, leading towards black hole formation. In the earlier work (see the review [21]), studies have been made of linear perturbations around the critical solution in terms of growing and decaying modes. In particular, the linear growing-mode index has been shown by Maison [27] to be equal to  $1/\gamma$ . Following

[27] (but with some variations), it is convenient to write the growing-mode amplitude for our quantity  $\bar{\Phi}$  as

$$\bar{\Phi}(\xi, \tau) - \bar{\Phi}_*(\xi) \propto (\delta - \delta_c) e^{\lambda_0 \tau} \psi_0(\xi), \quad (51)$$

where  $\bar{\Phi}_*(\xi)$  is the similarity solution and  $\tau = -\ln[(t_c - t)/t_H]$ . Note that increasing  $\tau$  corresponds to increasing  $t$ , and that

$$e^{\lambda_0 \tau} = [t_H/(t_c - t)]^{\lambda_0} \quad (52)$$

with  $\lambda_0$  being the index. Similarly, one can write the decaying-mode amplitude as

$$\bar{\Phi}(\xi, \tau) - \bar{\Phi}_*(\xi) \propto e^{\lambda_1 \tau} \psi_1(\xi), \quad (53)$$

(with no dependence on  $(\delta - \delta_c)$  being expected). We apply these to the peak value of  $\bar{\Phi}$ , i.e.  $(2M/R)_{\text{peak}}/2$ . In figure 6, we first plot (in the left frame) simulation results for  $(2M/R)_{\text{peak}}$  as functions of  $\tau$ , coming from a succession of runs with different values of  $(\delta - \delta_c)$  equally spaced in the log (decreasing successively by factors of 2 moving from left to right). The  $\log_e$  of the growing mode amplitude at the peak  $(\bar{\Phi} - \bar{\Phi}_*)_{\text{peak}}$  is then plotted against  $\tau$  in the right-hand frame. From the equal spacing of the curves in the rising part, one can immediately see the expected linear dependence on  $(\delta - \delta_c)$  for the growing mode. By making straight-line fits to the most linear segments of the growing and decaying parts of the curves, one can read off values of  $\lambda_0$  for the growing mode and  $\lambda_1$  for the decaying mode. (We have marked our straight-line fits with the dashed lines.) We find  $\lambda_0 = 2.81$  for the growing mode and  $\lambda_1 = -1.17$  for the decaying mode. Again following Maison [27], we anticipate that  $1/\lambda_0$  should be equal to  $\gamma$ , the index of the scaling law for  $M_{BH}$ . In fact, we have that  $1/\lambda_0 = 0.356$  which compares with  $\gamma = 0.3558$  as given by Maison for  $w = 1/3$  and our value of  $\gamma = 0.357$  as given in Paper 3. We should stress, however, that while  $\lambda_0 = 2.81$  was genuinely our best fit, we do not believe that it should be trusted to better than about  $\pm 2$  in the last digit.

## 5. Investigation of the effects of varying $w$ and the shape of the initial perturbation

In the literature on critical collapse, there has been discussion of the consequences of using “perfect fluids” having equations of state of the form  $p = we$ , with  $w$  taking values covering the range from 0 to 1 [27, 15]. Our own interest is strictly related to the possibility that critical collapse might actually occur under realistic circumstances, and a particular context for this arises in the case of the radiation fluids which dominated the universe at early times and could be reasonably approximated with an equation of state of the form  $p = we$  with  $w = 1/3$ . Investigation of similar equations of state with  $w \neq 1/3$  may be of interest in relation to this, for giving some indication of the effects of softening of the equation of state at the time of phase transitions, or stiffening due to some non-standard interactions. One needs to proceed with caution, however.

Standard simple fluids have pressure proportional to internal energy density, not to the *total* energy density (including also the rest-mass energy of the constituent particles).

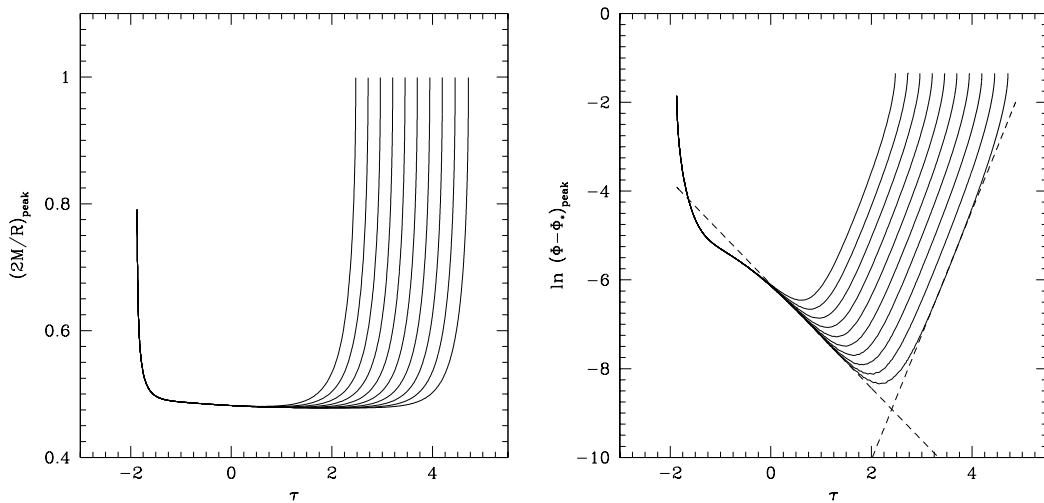


**Figure 6.** Plots for investigating growing and decaying perturbation modes around the similarity solution. See text for details.

The form  $p = we$  is relevant in the limit where the rest-mass energy becomes negligible compared with the kinetic energy of random motions (as for a radiation fluid). Using  $p = we$  for a perfect fluid with positive values of  $w$  different from  $1/3$  has doubtful physical motivation.

Having made that caveat, however, we now look at cases with  $w \neq 1/3$  with the aim mentioned above. We use exactly the same approach as that used for  $w = 1/3$ , even though there is some artificiality in doing this because of having the whole universe following an unusual equation of state and imposing initial conditions under those circumstances. If one were really considering in detail possible PBH formation with a variant equation of state, one would need a more sophisticated set-up than our present one. However, our aim here is just to get some general indications about the effect of varying  $w$ . We have studied a range of values for  $w$  between 0.01 and 0.6, checking on how the values of  $\gamma$  and  $\delta_c$  for the scaling laws varied with  $w$  and also with varying the shape of the initial perturbation. Regarding the hydrodynamics of the process: as  $w$  is increased, the features of the relativistic wind and the opening up of the void become progressively more extreme, and this eventually becomes very challenging for the adaptive scheme. It is because of this that we did not use values of  $w > 0.6$ . For the variant perturbation shapes, we used the forms of curvature profile given by equation (17) with  $\alpha \neq 0$ . The corresponding perturbations of the energy density, given by equation (19), are shown in figure 7 for the particular case  $w = 1/3$  and  $\delta = \delta_c$ , as an indication of the general behaviour. Varying  $\alpha$  in the range between 0 and 1 gives a centrally-peaked perturbation shape, while for  $\alpha$  greater than 1 it is off-centred.

With all of the cases which we studied ( $0.01 \leq w \leq 0.6$  and  $0 \leq \alpha \leq 5$ ) we found good scaling laws extending down to the smallest values of  $(\delta - \delta_c)$  for which we were able to make satisfactory calculations. The intermediate state and approximate

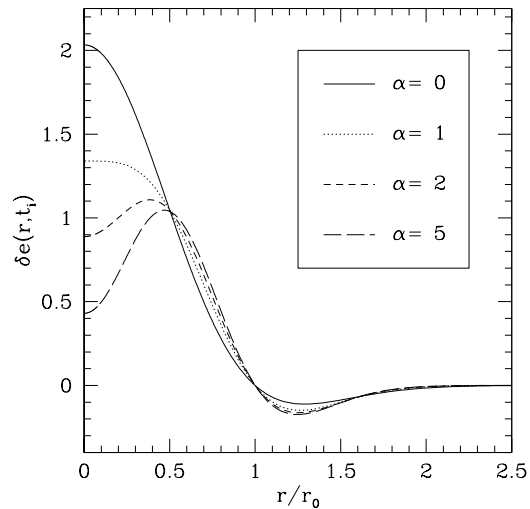


**Figure 7.** Different shapes of the energy-density perturbation obtained with different values of  $\alpha$ , for the particular case  $w = 1/3$  and  $\delta = \delta_c$ .

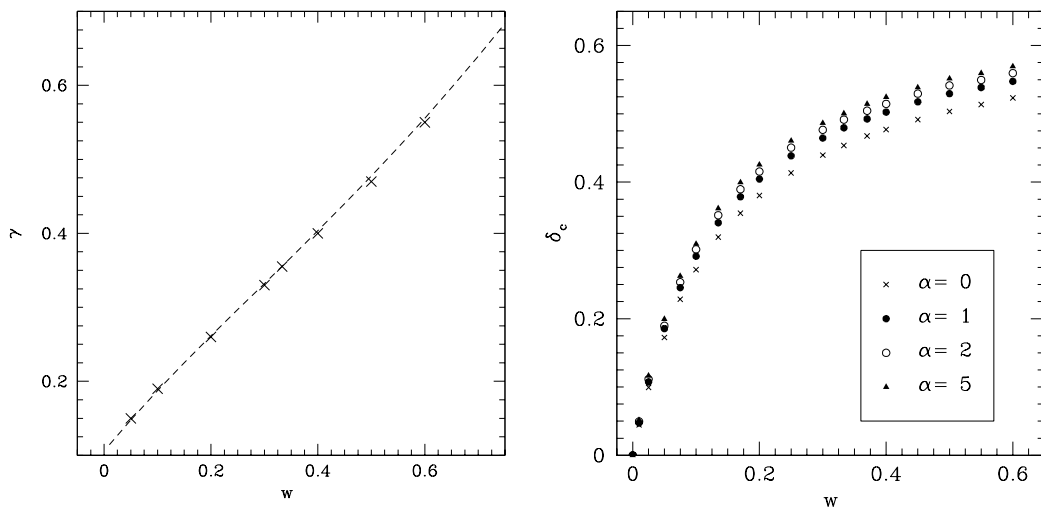


**Figure 8.** The left-hand plot shows the behaviour of  $\gamma$  as a function of  $w$  (with the dashed line indicating the corresponding results obtained semi-analytically by Maison [27]). The right-hand plot shows the behaviour of  $\delta_c$  as a function of  $w$ , as well as the variations depending on the shape parameter  $\alpha$  (these variations are negligible in the left-hand plot and so are not shown there).

similarity solution were clearly seen in all cases, with the value of  $(2M/R)_{peak}$  decreasing with decreasing  $w$ . Figure 8 shows our best-fit values of  $\gamma$  and  $\delta_c$  as functions of  $w$ . In the case of  $\gamma$ , the results obtained for different values of  $\alpha$  are indistinguishable on the scale of the plot, while for  $\delta_c$  small variations are seen. The results for  $\gamma$  are in good agreement with those previously obtained semi-analytically by Maison [27] (which are indicated here with the dashed line). Within the range shown, there is a roughly linear behaviour which is consistent with the limit of  $\gamma \rightarrow 0.106$  for  $w \rightarrow 0$  obtained by

Snajdr [28]. Regarding  $\delta_c$ , although the change with  $\alpha$  does not seem to be very large, it could be cosmologically relevant because the PBH mass spectrum is very sensitive to the precise value of  $\delta_c$ . It is therefore important to establish the connection between different inflationary models and the probabilities for different initial perturbation shapes, and more investigation of this should be made in future for getting a better understanding of the possible cosmological impact of PBHs. The plot indicates that among the profiles studied here, the simple Mexican hat (with  $\alpha = 0$ ) gives the lowest value of  $\delta_c$  and so the highest probability of forming PBHs. The relation between  $\delta_c$  and  $w$  confirms that any epochs in the early universe when the equation of state softens should be favourable for enhancing PBH production. One example of this could be the QCD phase transition, which has previously been discussed in connection with a PBH model for MACHOs [13].

Finally we want to comment here on one of our earlier results, in Paper 1, where we investigated critical collapse for a radiative fluid also in the presence of a cosmological constant  $\Lambda$ . At the time of Paper 1, our code was not able to get very close to the critical limit because of not yet having the AMR, and the lowest value of  $(\delta - \delta_c)$  that we were able to treat was around  $10^{-3}$ . In that regime we found that the presence of a cosmological constant was affecting the scaling law, giving a change in the value of  $\gamma$  in the sense of decreasing it with increasing (positive)  $\Lambda$ . Now, with the present AMR code, we have made similar calculations going down to much smaller values of  $(\delta - \delta_c)$  and have seen that this change in  $\gamma$  disappears as one gets closer to  $\delta_c$  (i.e. the gradients of the two scaling laws converge to the same value). The reason for this is clear: if  $\delta$  is very close to  $\delta_c$ , the mass of the black hole is small and the fluid densities involved in forming it are high. Under these circumstances, the energy density related to the cosmological constant becomes negligible in comparison with that of the collapsing fluid. This makes the gradient of the scaling law converge to the same value as without the cosmological constant when  $(\delta - \delta_c)$  is sufficiently small. However, the cosmological constant still makes a relevant (and growing) contribution on larger scales where the fluid density is lower.

## 6. Conclusions

Following on after our previous work investigating primordial black hole formation during the radiative era of the early universe, we have here investigated further the critical nature of the collapse in this context, focusing on the intermediate state, which appears in the case of perturbations close to the critical limit. We have examined the extent to which this follows a similarity solution, deriving and solving the set of equations describing a self-similar solution within the same foliation used for our simulations of black hole formation. This is a key issue, because the presence of a similarity solution is seen as an important characteristic feature of the general phenomenon of critical collapse. Also, we have presented results from calculations where the equation of state parameter  $w$  was allowed to take constant values different from the radiation value of  $1/3$ , with the aim of gaining further insight into our main case of interest, and have

studied the effect of using different perturbation shapes. Our calculations have been made using a purpose-built Lagrangian AMR code, starting with initial supra-horizon scale perturbations of a type which could have come from inflation and then following self-consistently both the formation of the black hole and the continuing expansion of the universe.

From our simulation results, we have found that the similarity solution does indeed emerge in this context as an attractor solution approached during the intermediate state. However, for runs with perturbations whose amplitude  $\delta$  is just above the critical value  $\delta_c$ , we observe it arising together with decaying and growing perturbation modes. First, the decaying mode is seen operating as the similarity solution is approached during the intermediate state but then the growing mode takes over, leading away from the intermediate state and the similarity solution, towards black hole formation. As expected, the index of the growing mode is found to be closely equal to  $1/\gamma$ , where  $\gamma$  is the exponent of the scaling law for the black-hole mass. During the time of the intermediate state, the range over which the similarity solution gives a good approximation to the simulation results becomes progressively larger, eventually extending over all of the contracting region and part of the surrounding evacuated region, up to the maximum in the velocity of the relativistic wind, corresponding to the deepest point of the surrounding semi-void. Further out, the simulation results diverge completely away from the similarity solution, transitioning onto the surrounding expanding universe. From our simulations for cosmological-type perturbations using values for  $w$  different from  $1/3$ , we have found that in every case, scaling-law behaviour persists down to the smallest values of  $(\delta - \delta_c)$  for which we were able to make satisfactory calculations, with the values obtained for the exponent  $\gamma$  being in almost perfect agreement with those obtained previously by other authors. The critical threshold amplitude  $\delta_c$ , the intermediate state compactness  $(2M/R)_{peak}$  and the scaling-law exponent  $\gamma$  all vary with  $w$  in a way which is easily understandable in view of  $w$  being the ratio between the pressure and energy density of the fluid.

## Acknowledgments

This work has been partly carried out within the award ‘‘Numerical analysis and simulations of geometric wave equations’’ made under the European Heads of Research Councils and European Science Foundation EURYI (European Young Investigator) Awards scheme, supported by funds from the Participating Organizations of EURYI and the EC Sixth Framework Programme. We gratefully acknowledge helpful discussions, during the course of this work, with a number of colleagues including Carsten Gundlach, Alexander Polnarev, Bernard Carr, Ian Hawke and Karsten Jedamzik, and IM thanks SISSA for giving him use of their facilities.

## References

- [1] Zel'dovich Ya.B. & Novikov I.D. 1966 *Astron.Zh.* **43** 758 [*Sov.Astron.* **10** 602 (1967)]
- [2] Hawking S.W. 1971 *MNRAS* **152** 75
- [3] Carr B.J. & Hawking S.W. 1974 *MNRAS* **168**, 399
- [4] Carr B.J. 1975 *Astrophys.J.* **201** 1
- [5] Nadezhin D.K., Novikov I.D. & Polnarev A.G. 1978 *Sov.Astron.* **22(2)** 129
- [6] Bicknell G.V. & Henriksen R.N. 1979 *Astrophys.J.* **232** 670
- [7] Novikov I.D. & Polnarev A.G. 1980 *Sov.Astron.* **24(2)** 147
- [8] Niemeyer J.C. & Jedamzik K. 1999 *Phys.Rev.D* **59** 124013
- [9] Shibata M. & Sasaki M. 1999 *Phys.Rev.D* **60** 084002
- [10] Hawke I. & Stewart J.M. 2002 *Class. Quantum Grav.* **19** 3687
- [11] Musco I., Miller J.C., Rezzolla L. 2005 *Class. Quantum Grav.*, **22**, 1405
- [12] Niemeyer J.C. & Jedamzik K. 1998 *Phys.Rev.Lett* **80** 5481
- [13] Jedamzik K. & Niemeyer J.C. 1999 *Phys.Rev.D* **59** 124014
- [14] Choptuik M.W. 1993 *Phys. Rev. Lett.* **70** 9
- [15] Neilsen D.W. & Choptuik M.W. 2000 *Class. Quantum Grav.*, **17**, 761
- [16] Polnarev A.G. & Musco I. 2007 *Class. Quantum Grav.*, **24**, 1405
- [17] Lifshitz E.M. & Khalatnikov I.M. 1963 *Usp. Fiz. Nauk.* **80**, 391 [*Sov. Phys. Usp.* **6**, 495 (1964)]
- [18] Lyth D.H., Malik K.A., Sasaki M. 2005 *JCAP* **May** 004
- [19] Musco I., Miller J.C., Polnarev A.G. 2009 *Class. Quantum Grav.*, **26**, 235001
- [20] Evans C.R. & Coleman J.S. 1994 *Phys. Rev. Lett.* **72** 1782
- [21] Gundlach C. & Martín-García J.M. 2007 *Living Rev. Relativity* **5**  
[<http://www.livingreviews.org/lrr-2007-5>]
- [22] Misner C.W. & Sharp D.H. 1964 *Phys.Rev* **136** B571
- [23] Misner C.W. 1969, in "Astrophysics and General Relativity, Volume 1, 1968 Brandeis University Summer Institute in Theoretical Physics" Eds. M. Chrétien, S. Deser and J. Goldstein (Gordon and Breach, New York), p.113
- [24] Hernandez W.C. & Misner C.W. 1966 *Astrophys.J.* **143** 452
- [25] Miller J.C. & Motta S. 1989 *Class. Quantum Grav.* **6** 185
- [26] Miller J.C. & Rezzolla L. 1995 *Phys.Rev.D* **51** 4017
- [27] Maison D. 1996 *Phys. Lett. B* **366** 82
- [28] Snajdr M. 2006 *Class. Quantum Grav.* **23** 3333